TU Delft

Delft University of Technology

Document Version
Final published version

Licence
CC BY

Citation (APA)
Kolff, M. J. C., Pool, D. M., Ricciardi, V., Heiderich, M., Zantner, F., & Shyrokau, B. (2026). A Model Predictive Control Algorithm for Matched Lateral/Yaw Motion. In A. Kemeny (Ed.), *Driving Simulation Conference DSC 2026 Europe* (Vol. 11)

Important note
To cite this publication, please use the final published version (if applicable).
Please check the document version above.

Copyright
In case the licence states “Dutch Copyright Act (Article 25fa)”, this publication was made available Green Open Access via the TU Delft Institutional Repository pursuant to Dutch Copyright Act (Article 25fa, the Taverne amendment). This provision does not affect copyright ownership.
Unless copyright is transferred by contract or statute, it remains with the copyright holder.

Sharing and reuse
Other than for strictly personal use, it is not permitted to download, forward or distribute the text or part of it, without the consent of the author(s) and/or copyright holder(s), unless the work is under an open content license such as Creative Commons.

Takedown policy
Please contact us and provide details if you believe this document breaches copyrights.
We will remove access to the work immediately and investigate your claim.

This work is downloaded from Delft University of Technology.

A Model Predictive Control Algorithm for Matched Lateral/Yaw Motion

Maurice Kolff[1], Daan M. Pool[2], Vincenzo Ricciardi[3], Martin Heiderich[3], Frank Zantner[3], Barys Shyrokau[1]

(1) Delft University of Technology, Faculty of Mechanical Engineering, section of Intelligent Vehicles, 2628 CD Delft, e-mail : {m.j.c.kolff, b.shyrokau}@tudelft.nl.
(2) Delft University of Technology, Faculty of Aerospace Engineering, section of Control & Simulation, 2629 HS Delft, e-mail : d.m.pool@tudelft.nl.
(3) Honda R&D Europe (Deutschland) GmbH, Vehicle Technology Research, 63073 Offenbach, Germany.

Abstract - *This paper describes a novel model-predictive control motion cueing approach for driving simulation. The simulator's lateral and yaw motions are explicitly matched through known relations from vehicle dynamics, rather than the state-of-the-art approach of optimizing for the lateral and yaw motion channels separately. To evaluate the implementation, three representative example motion systems are considered: (MS 1) a hexapod, (MS 2) a hexapod with a yaw-drive underneath, and (MS 3) a hexapod with a y-drive underneath. Offline, open-loop simulations for a driving scenario were compared objectively through the root-mean square difference. The results show the effectiveness of the matched approach compared to the state-of-the-art baseline approach without explicit matching. By purposefully reducing the motion in either the lateral or yaw direction, an improved motion reproduction compared to the state-of-the-art approach is achieved, which was confirmed by four drivers in a pilot study. While the presented approach requires further experimental validation, the matching of vehicle lateral and yaw motion may enable a leap towards vehicle dynamics-based motion cueing.*

Keywords: *Motion Cueing Algorithm, Model Predictive Control, Vehicle Dynamics*

Copyright: © 2026 by the authors.
Licensee Driving Simulation Association.
This article is an open access article distributed under the terms and conditions of the Creative Commons Attribution (CC BY) license (https://creativecommons.org/licenses/by/4.0/).
https://doi.org/10.82157/dsa/2026/9

1. Introduction

Over the last twenty years, Model-Predictive Control (MPC) Motion Cueing Algorithms (MCAs) (Dagdelen, et al., 2004; Jacumet, et al., 2026; Khusro, et al., 2020) have dominated motion cueing research and development in the field of driving simulation. The working principle of such algorithms is to optimize the simulator motion through a cost function, while respecting the workspace limitations through explicit optimization constraints. The typical approach in such algorithms is to optimize for the motion of the six motion channels (i.e., three specific forces and three rotational rates) separately. These channels are therefore considered independently in the optimization, such that the simulator motion is generally brought to these individual reference signals of the vehicle as closely as possible. Furthermore, different and independent weights are typically set for the different motion channels. This means that one typically only has limited control over the extent to which the relative magnitude between different motion channels, as present in the vehicle, is retained in the simulator.

In real-world driving, however, the six motion channels of the vehicle are not independent of each other. Most notably, in curve driving, the lateral acceleration and yaw rate are directly related through the vehicle's velocity. For motion cueing that is representative of real driving, drivers may therefore expect the same match between lateral acceleration and yaw rate as present in the real vehicle, even if the magnitudes of both motions are reduced. Especially in the expert evaluation of vehicles, ensuring motion magnitudes across different channels that match the real vehicle dynamics is crucial for valid simulator-based assessments.

Current MPC MCAs typically consider the lateral and yaw rate motion to be independent optimization channels (Hvitfeldt, Drugge, and Jerrelind, 2025; Jacumet, et al., 2026), such that this relative matching is not provided at all. If the lateral and yaw motion channels are independently optimized, there may thus be a resulting mismatch in the representation of the simulated vehicle dynamics. This can occur especially in a case where a motion system is able to provide a significant lateral specific force without the corresponding yaw motion, resulting in the sensation of understeering (too little yaw). In that case, it may be more beneficial to deliberately limit the lateral

specific forces provided in the simulator to match in magnitude with the provided yaw rate motion, and as a result, better correlation with the original vehicle's dynamics. Vice versa, simulators with large yaw motion and small lateral motion capabilities may create the sensation of oversteering (too much yaw), where it would be beneficial to purposefully reduce the yaw motion to match the lateral motion. Existing work has investigated additional control on sideslip dynamics of a vehicle, (Bruschetta, et al., 2018), and using a motion scaling approach (Hvitfeldt, Drugge, and Jerrelind, 2025). To the best of our knowledge, however, a general MPC implementation of magnitude-matched control between the lateral acceleration and yaw rate, without the need of explicit scaling relations, does not yet exist.

The contribution of this paper is to present a method to explicitly implement the matching between the lateral acceleration and yaw rate in an MPC cost function. The well-known vehicle dynamics relation between lateral acceleration and yaw is rewritten in terms of the lateral specific force rather than acceleration. It is then implemented as a reference tracking term in the MPC cost function. The paper provides an offline open-loop comparison of a state-of-the-art MPC (as the baseline) and the novel approach using the explicit vehicle dynamics "matching". For the evaluation, three motion systems are considered (MS 1: hexapod, MS 2: hexapod + yaw drive, MS 3: hexapod + y-drive) to demonstrate its functionality across a range of typical driving simulator motion systems with varying lateral and yaw motion workspaces. Apart from its successful implementation in curve driving (for which it was designed), the method is furthermore demonstrated to work on straight and inclined roads.

The structure of the paper is as follows. Section 2 derives the cost function formulation for the magnitude-matched lateral/yaw motion based on vehicle dynamics. Section 3 presents the simulation results for the different motion systems. A discussion is provided in Section 4. Finally, the paper is concluded in Section 5.

2. Method

2.1. Vehicle Dynamics

Considering vehicle dynamics, see Figure 1, the linear acceleration in the body frame B in the center of gravity can be calculated as (Jazar, 2025):

$$\begin{aligned} \boldsymbol{a}^B = \dot{\boldsymbol{u}} + \boldsymbol{\omega} \times \boldsymbol{u} &= \begin{bmatrix} \dot{u}_x \\ \dot{u}_y \\ \dot{u}_z \end{bmatrix} + \begin{bmatrix} \omega_x \\ \omega_y \\ \omega_z \end{bmatrix} \times \begin{bmatrix} u_x \\ u_y \\ u_z \end{bmatrix} \\ &= \begin{bmatrix} \dot{u}_x + u_z\omega_y - u_y\omega_z \\ \dot{u}_y - u_z\omega_x + u_x\omega_z \\ \dot{u}_z + u_y\omega_x - u_x\omega_y \end{bmatrix}, \end{aligned} \tag{1}$$

where $\boldsymbol{u}$ are the linear velocities of the body frame and $\boldsymbol{\omega}$ are its rotational rates. Hence, the vehicle lateral acceleration equals:

$$a_y^B = \dot{u}_y - u_z\omega_x + u_x\omega_z \approx \dot{u}_y + u_x\omega_z, \tag{2}$$

where the right-most expression holds for small u_z, i.e., for an even surface. The equation relates the lateral acceleration a_y and the yaw rate ω_z through the longitudinal velocity u_x and $\dot{u}_y$ (the time derivative of the lateral velocity u_y). These quantities apply to the vehicle's center of gravity, as indicated in Figure 1.

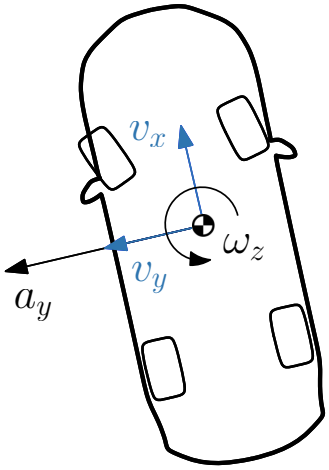


Figure 1: The vehicle system seen from the top, showing the relevant accelerations and velocities in the body reference frame around the center of gravity.

To provide fully matching motion between a_y^B and ω_z in the simulator, the relationship given by Eq. (2) must be respected. However, Eq. (2) cannot be directly incorporated into the MCA architecture. This is because the otoliths in the human vestibular system, located in the inner ear of the human body, are sensitive to specific forces, rather than accelerations. This makes the specific forces the relevant quantity for an MCA to reproduce. The specific forces may be considered as the combination of the accelerations and the reaction forces caused by gravity that acts on the driver via the seat (Stroosma, 2025). As a result, a tilting of the vehicle over a roll angle φ will thus also result in a gravity component in the body lateral specific force f_y^B.

In a real vehicle, a driver will thus perceive the linked dynamics of Eq. (2) between the lateral acceleration and yaw rate indirectly via the specific forces. Thus, in the simulator, the goal is to reproduce specific force and rotational rate motion that is matching via the vehicle relation of Eq. (2). Our approach is therefore to rewrite the vehicle dynamics relation of Eq. (2) to an equivalent form in terms of the specific forces and rotational rates, which may then be implemented in the MCA. We first consider the 3-element specific force vector of the vehicle, which may be calculated as:

$$\boldsymbol{f}^B = \boldsymbol{T}(\boldsymbol{\beta})(a^I + \boldsymbol{g}^I) = a^B + \boldsymbol{T}(\boldsymbol{\beta})\boldsymbol{g}^I, \tag{3}$$

with B the body system, I the inertial system, and where $\boldsymbol{\beta} = [\varphi,\ \theta,\ \psi]$, i.e., the Euler angles. The vector $\boldsymbol{g}^I = [0,\ \ 0,\ \ g]^\top$ represents the contribution of gravity. Finally, the rotation matrix represents the attitude of the vehicle:

$$\boldsymbol{T}(\beta) = \boldsymbol{R}_x^\top(\varphi)\,\boldsymbol{R}_y^\top(\theta)\,\boldsymbol{R}_z^\top(\psi), \tag{4}$$

with each rotation matrix $\boldsymbol{R}$ representing pure rotations around the given axis. The lateral specific force then equals:

$$f_y = \boldsymbol{c}_2\boldsymbol{f} = a_y^B + \boldsymbol{c}_2\boldsymbol{T}(\boldsymbol{\beta})\boldsymbol{g}^I, \tag{5}$$

where the role of the selector vector $\boldsymbol{c}_2 = [0,\ 1,\ 0]$ is

to select only the lateral specific force. We may now substitute Eq. (2) into Eq. (5):

$$f_y = \dot{u}_y + u_x \omega_z + \boldsymbol{c}_2 \boldsymbol{T}(\beta) \boldsymbol{g}^I. \tag{6}$$

This resulting equation is thus the specific force equivalent of the vehicle dynamics equation in Eq. (2). Note that this relation also remains true for a curved surface (non-zero roll φ and pitch θ angles) due to its definition in terms of the specific force rather than acceleration.

2.2. Simulator Control

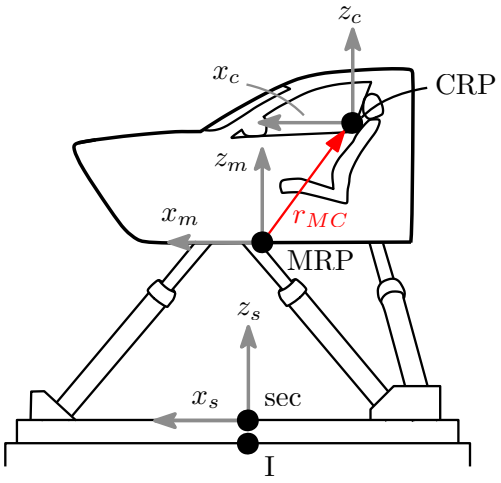


Figure 2: Simulator side view showing the relevant reference points and coordinate systems, adapted from (Kolff, et al., 2023).

Providing "matched" motion in terms of the vehicle dynamics relationship of Eq. (2) in the simulator thus implies constraining the simulator lateral specific force and yaw rate according to the relation of Eq. (6). The specific force cueing enabled by the simulator depends strongly on its kinematic configuration (Kolff, et al., 2023). In this paper, three relevant and representative driving simulator motion systems are considered:

- MS 1: A hexapod, the most widely adopted motion system, with a 12 cm stroke.
- MS 2: The same hexapod as MS 1, mounted on top of an additional $\pm 20°$ yaw drive (e.g., Jacumet, et al., 2025).
- MS 3: The same hexapod as MS 1, mounted on an additional ± 5 m y-drive, similar to the systems available at VTI (Jansson, et al., 2014), IKA (Wagener, et al., 2023), and Daimler (Cleij, et al., 2019).

These different motion systems are used to demonstrate the functionality of the lateral/yaw motion matching for different available workspaces. A schematic side view of the considered hexapod system is shown in Figure 2, showing the relevant reference points. Note that in the case of MS 2 and MS 3 the additional motion axes under the hexapod are represented by the movement of the reference point "sec" (*secondary*), to which the hexapod motion of the Motion Reference Point (MRP) is relative. This point is where the motion signals are defined. Relevant for the driver's perception is the Cueing Reference Point (CRP), approximating the location of the human vestibular system in the inner ear. The difference between the two reference points is denoted by the position vector r_{MC}. In further analysis, the simplifying case of $r_{MC} = [0,\ 0,\ 0]^\top$ is considered.

The specific forces generated by the motion system may be calculated as (Kolff, et al., 2023):

$$\begin{bmatrix} f_x^s \\ f_y^s \\ f_z^s \end{bmatrix} = \boldsymbol{R}_x^\top(\varphi^s)\, \boldsymbol{R}_y^\top(\theta^s)\, \boldsymbol{R}_z^\top(\psi^s) \left(\begin{bmatrix} a_x^s \\ a_y^s \\ a_z^s \end{bmatrix}_{hex} + \ldots \right. \\ \left. \underbrace{\boldsymbol{R}_z^\top(\psi_d^s) \begin{bmatrix} 0 \\ a_y^s \\ 0 \end{bmatrix}_{sec}}_{\text{MS 3 only}} + \begin{bmatrix} 0 \\ 0 \\ g \end{bmatrix} \right). \tag{7}$$

The superscript $(\cdot)^s$ here indicates that these are "simulator" signals. Note that Eq. (7) again highlights why the matching can indeed not be implemented directly on the simulator acceleration, as the relevant quantify for the reference tracking is the specific force, which may be reproduced as a combination of the simulator acceleration and cabin tilting (tilt-coordination, Stratulat, et al., 2011).

Similarly, the simulator rotational rates are calculated as (Kolff, et al., 2023):

$$\begin{bmatrix} \omega_x^s \\ \omega_y^s \\ \omega_z^s \end{bmatrix} = \begin{bmatrix} 1 & 0 & -\sin\theta^s \\ 0 & \cos\varphi^s & \sin\varphi^s \cos\theta^s \\ 0 & -\sin\varphi^s & \cos\varphi^s \cos\theta^s \end{bmatrix} \begin{bmatrix} \dot{\varphi}^s \\ \dot{\theta}^s \\ \dot{\psi}^s \quad \underbrace{+\, \dot{\psi}_{sec}^s}_{\text{MS 2 only}} \end{bmatrix}. \tag{8}$$

2.3. Cost Function Formulation

To integrate the vehicle dynamics relation, a typical MPC cost function formulation is used:

$$\mathcal{J}_{(k)} = \sum_{i=1}^{N_p} (\boldsymbol{y}_{(i,k)}^v - \boldsymbol{y}_{(i,k)}^s)^\top \boldsymbol{Q} (\boldsymbol{y}_{(i,k)}^v - \boldsymbol{y}_{(i,k)}^s) \\ + \sum_{i=1}^{N_p} \boldsymbol{x}_{(i,k)}^\top \boldsymbol{R} \boldsymbol{x}_{(i,k)}. \tag{9}$$

where the first term represents the reference tracking, with $\boldsymbol{y}_{(i,k)} \in [f_x,\ f_y,\ f_z,\ \omega_x,\ \omega_y,\ \omega_z]_{(i,k)}^\top$ and its weighting matrix $\boldsymbol{Q}$. The superscript $(\cdot)^v$ is added to indicate the reference vehicle signals. The second term, with the weight $\boldsymbol{R}$, penalizes the states $\boldsymbol{x}$ for washout behavior and added cost function convexity (Katliar, 2020). The MPC performs the optimization at each time step k, over elements i to a prediction horizon N_p. Especially in the real-time application of MPC, additional terms on the optimization input and the change in input are common (Jacumet, et al., 2026). However, these are not applied in the present analysis due to the offline optimization.

For the driver in the simulator to perceive motion that corresponds to the vehicle dynamics, we again consider and slightly rewrite Eq. (6):

$$-f_y^v + \dot{u}_y^v + u_x^v \omega_z^v + \boldsymbol{c}_2 \boldsymbol{T}(\beta^v) \boldsymbol{g}^I = 0. \tag{10}$$

The yaw rate and lateral specific force are now replaced by those of the simulator:

$$-f_y^s + \dot{u}_y^v + u_x^v \omega_z^s + \boldsymbol{c}_2 \boldsymbol{T}(\beta^v) \boldsymbol{g}^I = 0. \tag{11}$$

f_y^s and ω_z^s are physical motion signals produced by

the simulator, whereas the signals u_x^v and $\dot{u}_y^v$, as well as the vehicle attitude β^v, are visual motion signals, which thus remain in the vehicle system. Eq. (11) can be directly implemented in the reference tracking term of Eq. (9), to replace the independent baseline f_y^v tracking term:

$$\boldsymbol{y}^v_{(i,k)} - \boldsymbol{y}^s_{(i,k)} = \begin{bmatrix} f_x^v \\ \dot{u}_y^v + u_x^v\omega_z^s + \boldsymbol{c}_2\boldsymbol{T}(\boldsymbol{\beta}^v)\boldsymbol{g}^I \\ f_z^v \\ \omega_x^v \\ \omega_y^v \\ \omega_z^v \end{bmatrix}_{(i,k)} - \begin{bmatrix} f_x^s \\ f_y^s \\ f_z^s \\ \omega_x^s \\ \omega_y^s \\ \omega_z^s \end{bmatrix}_{(i,k)} . \tag{12}$$

Thus, the MCA still optimizes the specific forces in Eq. (7) and rotational rates in Eq. (8), but now aims to track the relation of Eq. (11) that matches the yaw rate simulator motion rather than the full lateral specific force of the vehicle reference data.

2.4. Solver

The optimization results presented in this paper used a pre-recorded drive, such that the optimization was performed offline. Hence, to analyze a best-case MPC result, the optimization therefore had full knowledge of all future states (Ellensohn, et al., 2019). The optimization problem was programmed in CasADi Python (Andersson, et al., 2019) and solved using Ipopt (Wächter and Biegler, 2006) at $\Delta t = 0.01$ s.

2.5. Scenario

The tested scenario involves representative handling with a sedan car on a two-lane test track. It first considers a left-right-left curve sequence (5 s to 15 s), followed by a straight section, and then slalom motion (30 s to 55 s). The total drive length was 60 s. The velocity remained constant around 80 km/h. In practice, the simulator performs fading in and out at the beginning and end of the simulation, respectively. Therefore, the novel matching reference tracking was not active in the fading in until $t_s = 5$ s, and the fading out after $t_e = 55$ s.

2.6. Verification

Considering the implementation of an additional tracking term rather than a constraint, the optimization is still allowed to find solutions that do not exactly satisfy the matching relation. This can especially occur when a (too) low weight on the f_y tracking term is used. Therefore, we quantify the difference between the target lateral specific force term to the actual generated specific force via the Root Mean Square Difference:

$$RMSD = \sqrt{\frac{1}{N}\sum_{i_s}^{N-i_e}\left[-f_y^s + \dot{u}_y^v + u_x^v\omega_z^s + \boldsymbol{c}_2\boldsymbol{T}(\boldsymbol{\beta}^v)\boldsymbol{g}^I\right]^2} \tag{13}$$

with N the number of samples, $i_s = t_s/\Delta t$, and $i_e = t_e/\Delta t$. Considering the present case of open-loop optimization, we may set $N = N_p$.

3. Results

3.1. Objective Evaluation

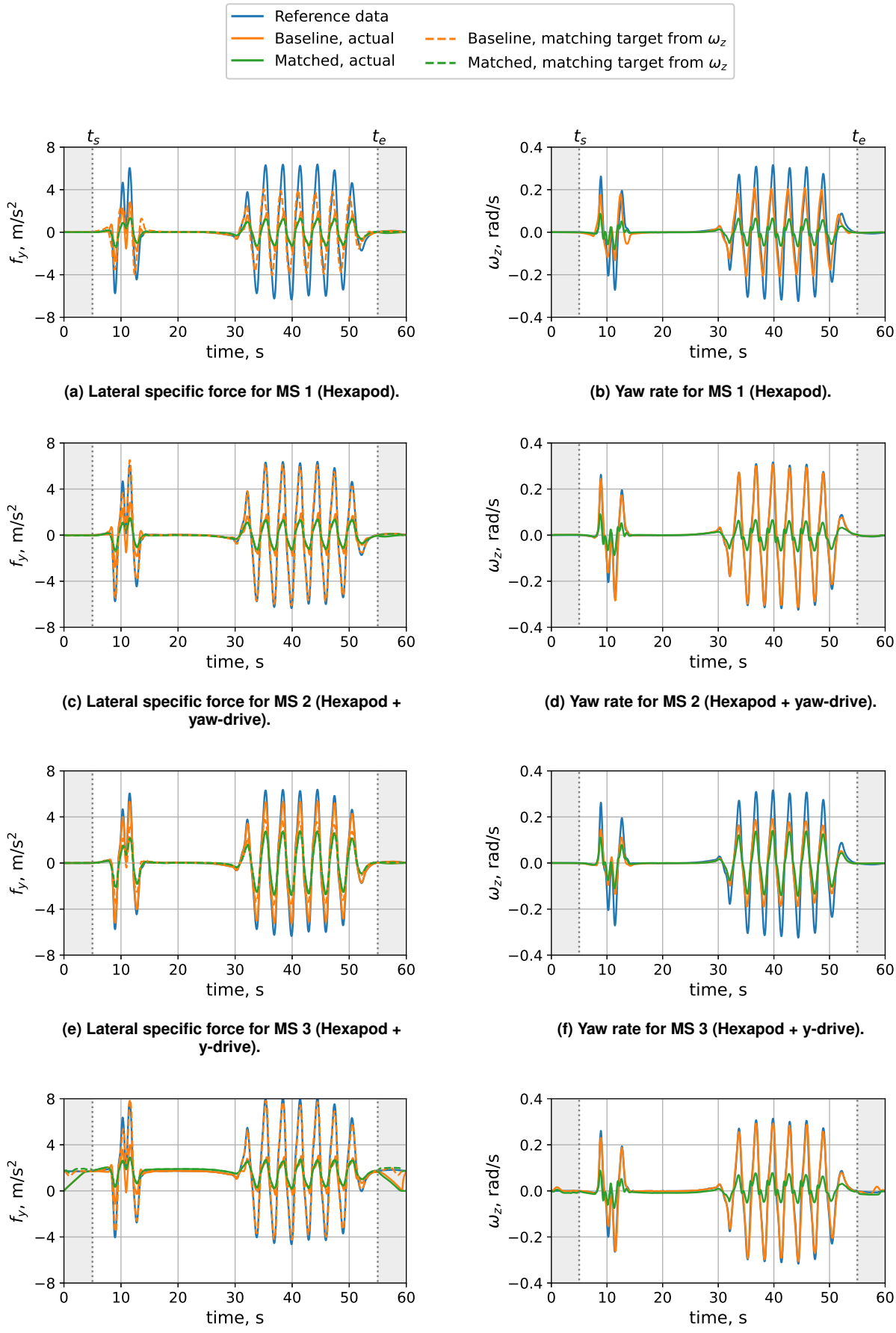
The results for the three motion systems are shown in Figure 3a-3f. The reference vehicle data (blue) are tracked by both the “baseline” and “matched” MPC variants, which are not able to fully reproduce the reference data, as expected due to the limited available workspaces. The orange lines represent the baseline MPC, i.e., without the matching tracking term active. Furthermore, the orange dashed lines in the lateral specific force plots (left column) represent what the lateral specific force *should have been* based on the yaw rate (right column), if matching motion were provided. From the difference between the solid and dashed lines it is evident that the baseline method does not provide matching motion.

The green lines show the outputs of the MPC *with* the matching tracking term. The term was not active in the grey shaded areas (see Section 2.5). Again the dashed lines are plotted to represent the matching target, but they are mostly not visible as they correspond exactly to the matched MPC’s actual lateral specific force motions. Qualitatively, this thus shows that matching motion is indeed provided.

The matching method is also seen to be effective across the considered variety in motion systems. For example, for MS 2 with the additional yaw drive, the system strongly reduces the yaw motion (Figure 3d) below what the workspace actually allows to match the limited available lateral motion (Figure 3c). Furthermore, for MS 3 with the additional y-drive for lateral motion, the optimization deliberately reduces the available lateral motion (Figure 3e) to match with the limited available yaw motion (Figure 3f).

An explicit quantitative comparison of the achieved lateral specific force/yaw motion match is shown in Figure 4, with the actual lateral specific force f_y^s on the y-axis and the matching target on the x-axis. The blue data represents the vehicle data, which indeed indicates perfectly matched motion between the two quantities, as expected. If matched simulator motion is provided, it should thus also lie on this straight $45°$ line. Here the efficacy of the MPC with matching tracking (green) is clearly visible compared to the baseline MPC (orange). Furthermore, the RMSD (see figure legends) strongly decreases from 1.02 to $5 \cdot 10^{-4}$ (MS 1), from 0.89 to $1.23 \cdot 10^{-3}$ (MS 2), and from 1.13 to $5.11 \cdot 10^{-4}$ (MS 3), when including the matching term. This confirms that the novel approach effectively achieves matching motion. The RMSD of the vehicle reference data is shown for completeness; it equals $2.98 \cdot 10^{-3}$.

A fourth case is considered where the vehicle drives the same slalom road, but with a constant $10°$ inclination of the road, which leads to a constant roll angle. This creates a constant offset in the vehicle specific force, as shown in Figure 3g, while not affecting the yaw rate (Figure 3h). As the matching relation in Eq. (11) accounts for any effects of the vehicle orientation due to the term $\boldsymbol{c}_2\boldsymbol{T}(\beta^v)\boldsymbol{g}^I$, the proposed matched MPC is effectively able to handle the additional road inclination and will still provide matching motion. This is further shown in Figure 4d, where the data are shifted to the right by $\boldsymbol{c}_2\boldsymbol{T}(\beta^v)\boldsymbol{g}^I$ due to the road inclination, and by the same amount upwards in f_y^s due



(a) Lateral specific force for MS 1 (Hexapod).

(b) Yaw rate for MS 1 (Hexapod).

(c) Lateral specific force for MS 2 (Hexapod + yaw-drive).

(d) Yaw rate for MS 2 (Hexapod + yaw-drive).

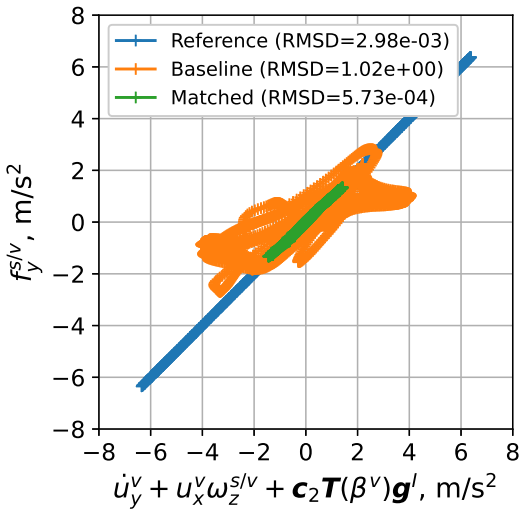
(e) Lateral specific force for MS 3 (Hexapod + y-drive).

(f) Yaw rate for MS 3 (Hexapod + y-drive).

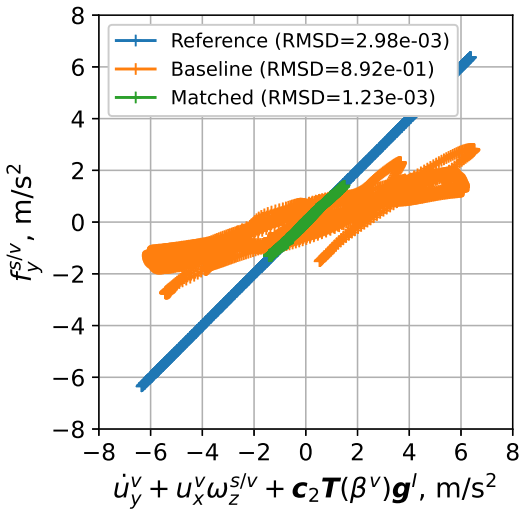
(g) Lateral specific force for MS 2 (Hexapod + yaw-drive), with 10° roll inclination in reference vehicle data.

(h) Yaw rate for MS 2 (Hexapod + yaw-drive), with 10° roll inclination in the reference vehicle data.

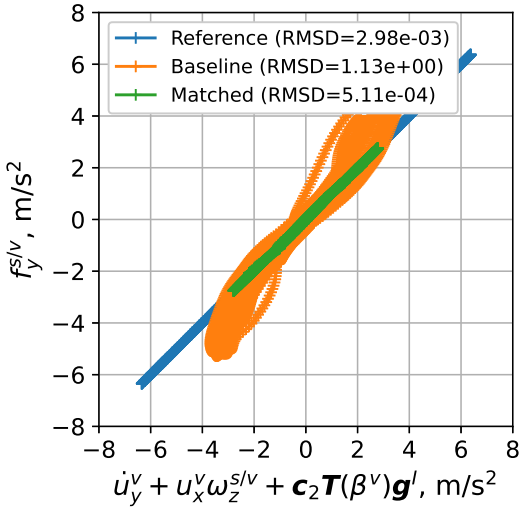
Figure 3: Optimization outputs for the baseline MPC (orange solid lines) and the MPC with the matching cost function (green solid lines), compared to the reference vehicle data (blue solid lines). Dashed lines indicate the matching lateral motion corresponding on the yaw rate. The grey areas were excluded from further analysis.



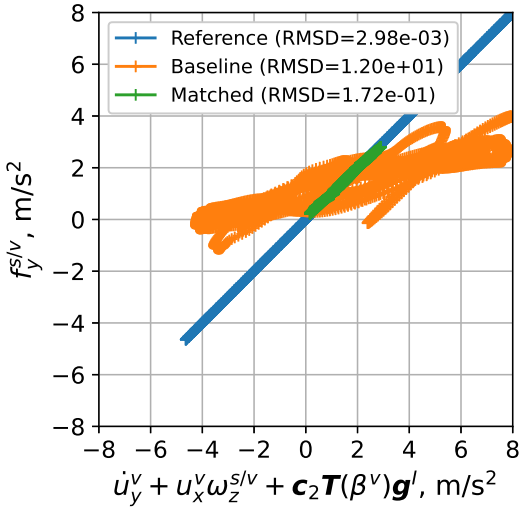
(a) Hexapod (MS 1).



(b) Hexapod + yaw-drive (MS 2).



(c) Hexapod + y-drive (MS 3).



(d) Hexapod + yaw-drive (MS 2), with 10° roll inclination in reference data.

Figure 4: Verification results of the optimization for the baseline MPC (orange) and the MPC with the matching tracking (green), compared to the baseline data (blue).

to the simulator rolling to reproduce the resulting specific force. The matching relation is thus valid, visible by the 45° blue and green lines. This shows that the matching MPC method is not restricted to fully flat road surfaces, but can directly handle a large variety of realistic road geometries.

3.2. Workspace Management

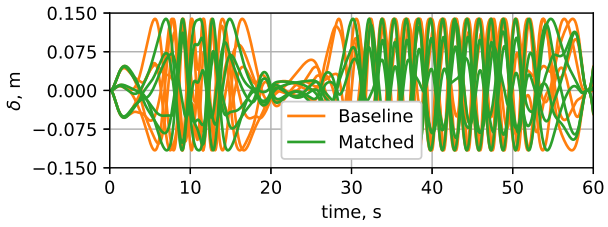
Figure 5 shows the time traces of the motion subsystems for the four conditions. In all four cases, the added matching provides a different workspace utilization in the hexapod. The magnitude of the hexapod stroke utilization is, however, similar. Larger differences are present in the yaw drive signals (Figures 5c and 5g), which are strongly reduced in magnitude in the matched approach. Overall, this shows an improved workspace management of the novel matched approach.

3.3. Subjective Evaluation

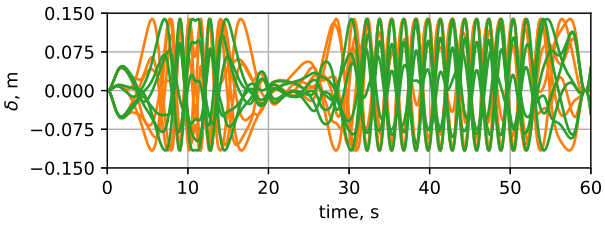
The baseline and matching MPCs were tested in a pilot study. All four drivers from TU Delft subjectively preferred the matching MPC over the baseline version. A larger controlled experiment is planned to systematically investigate the subjective differences between the two methods.

4. Discussion

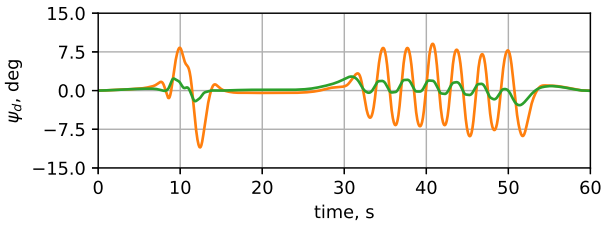
The main contribution of this paper is to propose a method that can enable matching lateral specific



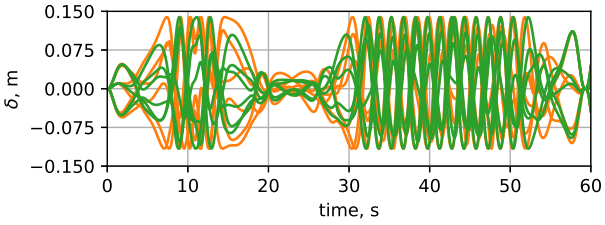
(a) MS 1: hexapod



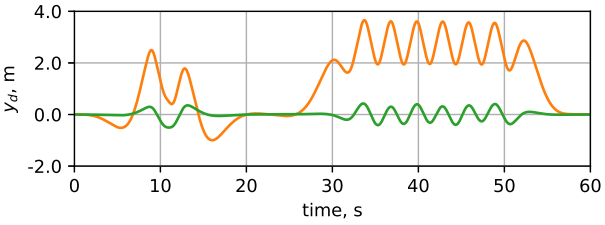
(b) MS 2: hexapod



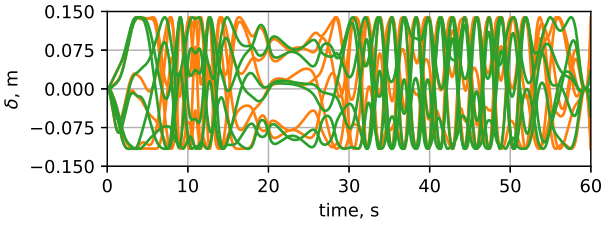
(c) MS 2: yaw-drive



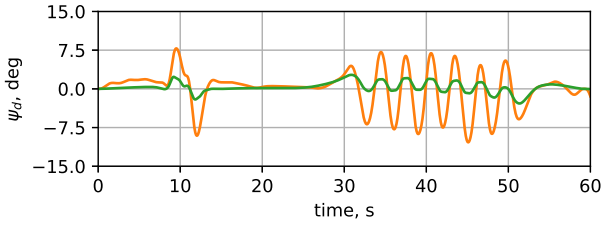
(d) MS 3: hexapod



(e) MS 3: y-drive



(f) MS 2, with 10° roll inclination in reference data: hexapod.



(g) MS 2, with 10° roll inclination in reference data: yaw-drive.

Figure 5: Workspace utilization of the four tested conditions.

force and yaw rate motion in MPC MCAs. The purpose of this is to provide motion that is more representative of real vehicle dynamics, where both motions are naturally linked. While providing more realistic motion cues to the driver, the workspace usage is reduced. The implemented methods are not only valid in curve driving; its general formulation describes the lateral motion at all times, also for straight driving. In that case, the lateral specific force will simply equal the term $\boldsymbol{c}_2\boldsymbol{T}(\beta^v)\boldsymbol{g}^I$, which is then only dependent on the inclination of the road. This provides a novel MPC approach that, without any added computational cost, remains closer to the vehicle dynamics than state-of-the-art MPC MCAs, while reducing the workspace usage. The proposed methods also suggest that always using the full workspace may not be beneficial if, as a result, the motion does not match anymore. The matching MPC thus speaks in favor of simulator systems that can provide additional lateral *and* yaw motion, rather than only emphasizing the motion in one of these.

No direct limitations were observed in the implementation of the matching MPC; the amount of tunable parameters remains the same and the optimization time was unaffected. Further adaptations of the reference data (e.g., due to the reference point shift between the CRP and MRP, as well as vestibular system model integration) can be relatively easily obtained by expressing Eq. (11) accordingly. However, significant future work is required in several directions. Whereas the presented methods have been developed within an MPC framework, the extension to real-time MPC with matched motion remains to be made. Furthermore, while the matching MPC was found to be preferred in small pilot study, the presented methods require a more thorough subjective

evaluation to prove the preference of the matched MPC.

Current proxy methods of subjective evaluations through objective metrics (e.g., Grottoli, et al., 2019; Kolff, et al., 2024) also follow the same paradigm as the baseline MPC in this paper, where each channel is treated separately and fully independent of all others. Such metrics would thus, also in our presented results, favor the baseline MPC, as it will always provide objectively better tracking in the lateral specific force and yaw rate channels. The lack of considering the matching in current quality metrics may explain the disputed role regarding the beneficial effect of yaw motion on subjectively rated motion quality (Hogema, Wentink, and Bertollini, 2012; Kolff, et al., 2024). Yaw motion may be beneficial, but *only* if it matches in shape and magnitude with the perceived lateral motion. To be able to then show the true benefits of the matching MPC proposed in this paper, an improvement in the existing metrics that can account for the quality of the matching would be necessary.

5. Conclusion

This paper presented a novel method to explicitly match the lateral and yaw motion in driving simulators based on the well-known vehicle dynamics relation between these dynamic states. This relation was integrated in an MPC architecture and simulated offline (playback) in a combined slalom and double lane change scenario. The simulation results, for three representative driving simulator motion system architectures (MS 1-3), show the effective implementation of the matching reference tracking. Verifiably matching motion as a result is obtained, while also reducing the workspace usage. The matching MPC is especially relevant for simulators where one of the relevant motion channels (lateral or yaw) is strongly limited compared to the other (i.e., our MS 2 and MS 3). The matched MPC then purposefully reduces the motion in the other channel to provide a less strong, but matching, combination of lateral and yaw motion compared to the baseline MPC approach. Furthermore, by implementing the matching term on the level of the specific force, the MPC can effectively provide matching motion even on inclined roads. An informal pilot study revealed the preference of the matching MPC of four drivers, although further and more extensive subjective testing is necessary to fully prove its efficacy. Overall, the proposed approach provides a first key step towards vehicle dynamics-based motion cueing, rather than optimization of all motion channels separately. This may greatly improve the motion cueing especially for expert evaluations and lead to more effective expert testing of vehicle dynamics in motion-based driving simulators.

References

Andersson, J. A. E., Gillis, J., Horn, G., Rawlings, J. B., and Diehl, M., 2019. CasADi – A software framework for nonlinear optimization and optimal control. *Mathematical Programming Computation*, 11(1), pp. 1–36. doi: 10.1007/s12532-018-0139-4.

Bruschetta, M., Mendola, D. L., Beghi, A., and Minen, D., 2018. An MPC based Motion Cueing Algorithm with side slip dynamics. In: *Proceedings of the Driving Simulation Conference 2018 Europe VR*. Antibes, France, pp. 55–59.

Cleij, D., Venrooij, J., Pretto, P., Katliar, M., Buelthoff, H. H., Steffen, D., Hoffmeyer, F., and Schöner, H.-P., 2019. Comparison between filter- and optimization-based motion cueing algorithms for driving simulation. *Transportation Research Part F: Traffic Psychology and Behaviour*, 61, pp. 53 –68. doi: 10.1016/j.trf.2017.04.005.

Dagdelen, M., Reymond, G., Kemeny, A., Bordier, M., and Maïzi, N., 2004. MPC Based Motion Cueing Algorithm: Development and Application to the ULTIMATE Driving Simulator. In: *Proceedings of the Driving Simulation Conference 2004 Europe*. Paris, France, pp. 221–233.

Ellensohn, F., Venrooij, J., Schwienbacher, M., and Rixen, D., 2019. Experimental evaluation of an optimization-based motion cueing algorithm. *Transportation Research Part F Traffic Psychology and Behaviour*, 62, pp. 115–125. doi: 10.1016/j.trf.2018.12.004.

Grottoli, M., Cleij, D., Pretto, P., Lemmens, Y., Happee, R., and Bülthoff, H. H., 2019. Objective evaluation of prediction strategies for optimization-based motion cueing. *Simulation*, 95(8), pp. 707–724. doi: 10.1177/0037549718815972.

Hogema, J., Wentink, M., and Bertollini, G., 2012. Effects of Yaw Motion on Driving Behaviour, Comfort and Realism. In: *Proceedings of the Driving Simulation Conference 2012 Europe*. Paris, France, pp. 149–158.

Hvitfeldt, H., Drugge, L., and Jerrelind, J., 2025. Motion cueing scaling for planar vehicle dynamics and body slip feedback. *Vehicle System Dynamics*, pp. 1–23. doi: 10.1080/00423114.2025.2497849.

Jacumet, R., Kolff, M., Venrooij, J., Schwienbacher, M., Wagner, S., Wollherr, D., Leibold, M., Pool, D. M., and Mulder, M., 2026. A Review on Optimization-Based Motion Cueing Algorithms for Driving Simulation. *IEEE Transactions on Intelligent Transportation Systems*, pp. 1–25. doi: 10.1109/TITS.2026.3661819.

Jacumet, R., Wetzel, J., Wagner, S., Schwienbacher, M., Wollherr, D., and Leibold, M., 2025. Optimization-based Motion Cueing Algorithm for Worst Case Maneuvers in Driving Simulation. In: *Proceedings of the Driving Simulation Conference 2025 Europe*. Stuttgart, Germany, pp. 163–168.

Jansson, J., Sandin, J., Augusto, B., Fischer, M., Blissing, B., and Källgren, L., 2014. Design and performance of the VTI Sim IV. In: *Proceedings of the Driving Simulation Conference 2014 Europe*. Paris, France, pp. 128–138.

Jazar, R. N., 2025. *Vehicle Dynamics: Theory and Application*. 4th ed. Springer New York, NY.

Katliar, M., 2020. Optimal control of motion simulators. PhD Dissertation. Albert-Ludwigs-Universität Freiburg.

Khusro, Y. R., Zheng, Y., Grottoli, M., and Shyrokau, B., 2020. MPC-based motion-cueing algorithm for a 6-DOF driving simulator with actuator constraints. *Vehicles*, 2(4), pp. 625–647.

Kolff, M., Venrooij, J., Schwienbacher, M., Pool, D. M., and Mulder, M., 2023. The Importance of Kinematic Configurations for Motion Control of Driving Simulators. In: *IEEE 26th International Conference on Intelligent Transportation Systems*. Bilbao, Spain, pp. 1000–1006. doi: 10.1109/ITSC57777.2023.10422127.

Kolff, M., Venrooij, J., Schwienbacher, M., Pool, D. M., and Mulder, M., 2024. Reliability and Models of Subjective Motion Incongruence Ratings in Urban Driving Simulations. *IEEE Transactions on Human-Machine Systems*, 54(6), pp. 634–645. doi: 10.1109/THMS.2024.3450831.

Stratulat, A., Roussarie, V., Vercher, J., and Bourdin, C., 2011. Does tilt/translation ratio affect perception of deceleration in driving simulators? *Journal of Vestibular Research: Equilibrium & Orientation*, 21(3), pp. 127–139. doi: 10.3233/VES-2011-0399.

Stroosma, O., 2025. Understanding Motion Cueing: Two Sides of Newton's Second Law. In: *AIAA SCITECH 2025 Forum*. Orlando, FL, pp. 1–11. doi: 10.2514/6.2025-0977.

Wächter, A. and Biegler, L., Mar. 2006. On the Implementation of an Interior-Point Filter Line-Search Algorithm for Large-Scale Nonlinear Programming. *Mathematical programming*, 106, pp. 25–57. doi: 10.1007/s10107-004-0559-y.

Wagener, N., Russ, F., Beckmann, J., Legran, P., and Eckstein, L., 2023. ika's highly dynamic driving simulator. In: *Product Solution Book of the Driving Simulation Conference 2023 Europe*. Antibes, France, pp. 103–104.